TRANSMISSION ZERO DESIGN GRAPH FOR DUAL-MODE DUAL-BAND FILTER WITH PERIODIC STEPPED-IMPEDANCE RING RESONATOR

Y.-C. Chiou and P.-S. Yang

Institute of Communication Engineering
National Chiao Tung University
Taiwan

J.-T. Kuo

Department of Electronic Engineering
Chang Gung University
Taiwan

C.-Y. Wu

Institute of Communication Engineering
National Chiao Tung University
Taiwan

Abstract—Compact dual-mode dual-band bandpass filters are realized with a single periodic stepped-impedance ring resonator. Neither extra resonator nor substrate layer is required for implementing the second passband. Based on the transmission line theory, a transmission zero design graph consisting of the transmission zeros together with the resonant frequencies of the resonator is developed against the space separation angle between the input and output ports. Based on this graph, when the line-to-ring feed structure is implemented, the space angle can be determined for the dual-mode dual-band design with designated zeros near the two passbands. It is believed that this is the first design graph for designating the transmission poles and zeros of a dual-mode ring resonator filter before the excitation structure is realized. Three dual-mode dual-band bandpass filters are carried out for demonstration. All circuits occupy only 60% of the area of the conventional ring resonator bandpass filter

at the first frequency. Measured results of experimental circuits show good agreement with simulated responses.

1. INTRODUCTION

Transmission zeros are attractive in microwave bandpass filter design. Transmission zeros near the passband are particularly useful in a down-conversion mixer for rejecting the image frequency. The ring resonator bandpass filter has such attractive feature since two transmission zeros can be generated on both sides of the passband [1–7]. There have been a series of innovative analysis, design and realization of the ring resonator filters. The hexagonal loop resonator in [2] can be used to design triple-mode filters with a pair of transmission zeros close to the passband. In [3], a line-to-ring structure is used to offer sufficient coupling for circuit synthesis. With suitable perturbation and input/output design, the filter may possess tunable transmission zeros and keep the bandwidth constant at the same time [4]. In [5], the resonant frequencies of the ring with a perturbation are analyzed based on the transmission-line theory. In [6], the periodic stepped-impedance ring resonator is contrived to have a dual-mode characteristic with compact circuit area and wide upper stopband. In [7], the ring resonator occupies only 19.3% of the area of a conventional ring. Note that these dual-mode ring resonator filters involve only a single passband.

Recent development of commercial wireless systems has created a need of dual-band or tri-band devices, including antennas [8–10], impedance transformers [11, 12] and bandpass filters [13–22]. The multi-band circuits can be realized by multi-mode resonators [13]. In [14], a novel dual-band bandpass filter is implemented with meander-loop resonator and complement split-ring resonator defected ground structure, operating at respective passbands. In [15], dual-band bandpass filters are realized using slotted ground resonator structures. The resonators allow the back-to-back and face-to-face embedding configuration, hence, greatly reduces the physical circuit size. The dual-mode dual-band bandpass filters can be realized using two elements resonating at designated frequencies [16, 17] or a single element with separated resonances [18–21]. In [16], a stacked-loop structure is used to design dual-mode dual-band bandpass filters. The circuit consists of two dual-mode loop resonators and each resonator controls one passband. This idea is extended to an alternative dual-band filter excited with CPW feed lines [17]. In [18], a dual-band bandpass filter is realized by a dual feeding structure. The two passbands are designed individually and several transmission zeros

are created. So far, it is still challenging to design dual-mode dual-band circuits with a single resonating element. In [19], the filter has a tunable second passband. In [20], the ring resonator is implemented by a cascade of several microwave C-sections. In [21, 22], the inner peripheral of the ring resonator is tapped with a circular open stub array. The stub length controls the separation between the two center frequencies.

This paper extends the use of the periodic stepped-impedance resonator in [6] to development of dual-mode dual-band filters. The resonator is treated as a dual-frequency element and perturbations are used to control the two resonances at each designated frequency. A new transmission zero design graph is devised based on the transmission theory. In comparison with [22], the advantage of this approach is that the proposed design graph clearly indicates the relationship among the two bandwidths, positions of the transmission zero on both sides of the passbands, and the space angle between the input/output ports. This will facilitate the circuit realization for design of all single-ring bandpass filters. For example, when the zeros are allocated, then the space angle between the input/output ports can be determined, and vice versa. Note that the allocation of the transmission zeros is usually an important specification for bandpass filter design. Three dual-mode dual-band filters are fabricated and measured for validation of our idea. For two of the three realizations, two transmission zeros are created on both sides of each passband, ensuring the high selectivity of the proposed structure. Finally, the measured results are compared with the simulated counterparts.

2. PROPERTIES OF PERIODIC STEPPED-IMPEDANCE RESONATOR

As described in [6], the ring peripheral consists of interlaced hi-Z and low-Z sections. Let N denote the number of periods in the ring. Fig. 1 shows two such rings with $N = 8$ and 6 of which the hi-Z and low-Z sections have characteristic impedances Z_1 and Z_2 and electric lengths θ_1 and θ_2, respectively. It can be validated that $\theta_1 + \theta_2 = 2\pi/N$ at the first resonant frequency.

The perturbation Z_3 in the plane of symmetry PQ is used to split off the degenerate modes. Two additional patches denoted by Z_p are also incorporated for perturbation. Based on the approach in [6], the resonant spectrum of the resonators can be readily obtained. Fig. 2 plots the split up modal frequencies f_{na} and f_{nb} ($n = 1 \sim 3$) against θ_2 for the resonators with $R = Z_1/Z_2 = 3$ and $R' = Z_1/Z_3 = 1.2R$ for $N = 4$ and 6, and $R = 3$ and $R' = 0.5R$ for $N = 8$. Note that f_{na} and

f_{nb} are calculated by treating the PQ plane as an electric and magnetic wall, respectively. All frequencies are normalized with respect to the fundamental frequency of a uniform ring resonator, f_o.

For $N = 6$ and 8, one can observe that f_{1a} and f_{1b} have a close distance and so f_{2a} and f_{2b} do. Thus both resonators can be used as building blocks of dual-mode dual-band bandpass filters. The center frequency f_i, $i = 1$ or 2, is then the arithmetic mean of f_{ia} and f_{ib}. On the other hand, for $N = 4$, f_{2a} in general has a considerable separation from f_{2b}, as f_{1a} does from f_{1b} for $N = 2$ in [6]. Similar separation between f_{3a} and f_{3b} for the resonator with $N = 6$ can be observed. This reflects the fact that if the leading four resonant frequencies are required for the two resonances in each of the two bands, N should be greater than 4. It explains why resonators with $N = 2$ and 3 are not used here. However, we will apply a special arrangement to resonator with $N = 4$ to meet the dual-band application. Note that the minimal circuit area requires that $\theta_1 = \theta_2 = \theta$ where f_i has its lowest value.

Figure 3 investigates the changes of f_{na} and f_{nb} and of ratios f_2/f_1 and f_3/f_1 with respect to variation of R for resonator with $N = 8$. The purpose of the ratio f_3/f_1 is to check the unwanted resonance next to the second passband. One can see that all resonances shift down to lower frequencies as R is increased. The ratio f_2/f_1 moves from 2.0 to 1.89 when R is increased from 1 to 8.

3. TRANSMISSION ZERO DESIGN GRAPH

Traditional ring resonator filters have two transmission zeros on both sides of the passband when the space between the input and output
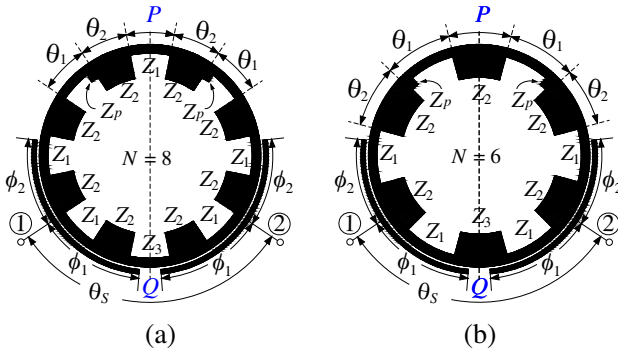

(a)   (b)

Figure 1. Periodic stepped-impedance ring resonators with line-to-ring feeds. (a) $N = 8$. (b) $N = 6$.
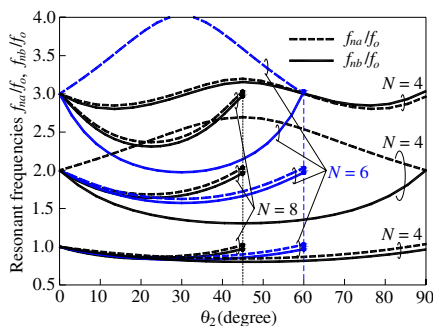
Figure 2. Resonant spectrum of the resonators. $R = 3$ and $R' = 3.6$ for $N = 6$ and 4. $R = 3$ and $R' = 1.5$ for $N = 8$. f_o is the fundamental frequency of a uniform ring. $\theta_1 = 2\pi/N - \theta_2$.
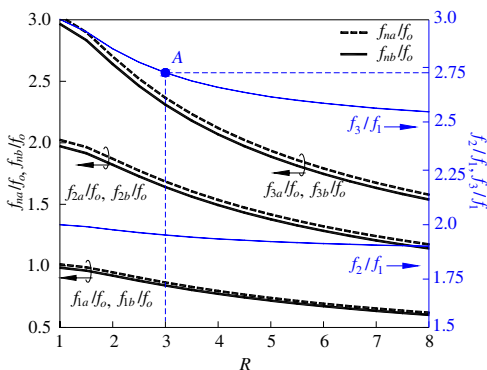

Figure 3. f_{na}, f_{nb}, f_2/f_1 and f_3/f_1 versus R. $N = 8$, $R' = 0.5R$.

lines is $90°$ [5]. These zeros are attractive since they greatly improve the frequency selectivity of the filter. The transmission line theory can be employed to find these zeros as follows. By letting the lengths of lower (ϕ_1) and upper (ϕ_2) arms of the line-to-ring structure be zero and attaching the input and output ports directly to the ring, the input admittances Y_{ine} (PQ plane open circuit) and Y_{ino} (PQ plane short-circuited) can be derived. The transmission zeros can be obtained by solving $Y_{ine} = Y_{ino}$. Apparently, the roots will be functions of θ_S, i.e., the spatial angle between the input and output ports.

Figure 4 draws f_{na}, f_{nb} and the transmission zeros f_{mz} as functions of θ_S for $N = 8$, where m is a positive integer. All these data are calculated by a root-searching program. Obviously, all f_{na} and f_{nb} will be independent of θ_S, since they are natural frequencies of the
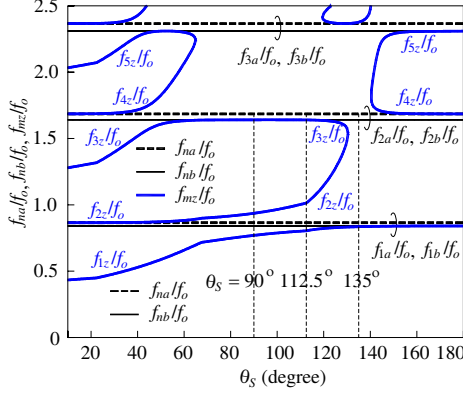
Figure 4. Transmission zero design graph for the resonator with $N = 8$. $R = 3$, $R' = 0.5R$.

resonator and will not be affected by any excitation. The transmission zeros, however, can be adjusted by tuning θ_s. It can be observed that there are two zeros on both sides of the two split-up degenerate modes. For the first passband, it suggests θ_S be between $65°$ and $115°$, since the passband may be affected when f_{mz} is too close to f_{na} or f_{nb}. It is interesting to note that when $\theta_S = 90°$, the first passband will be symmetric about f_1 since f_{1z} and f_{2z} are symmetrically allocated on both sides of the passband.

When $\theta_S < 60°$ and $\theta_S > 120°$, f_{1z} and f_{2z} are close to f_{1b} and f_{1a}, respectively. Also, f_{3z} and f_{4z} have a close proximity to f_{2b} and f_{2a} as $55° < \theta_S < 125°$ and $\theta_S < 40°$ or $\theta_S > 140°$. When $\theta_S = 180°$, f_{1z} and f_{4z} are in near neighborhoods of f_{1b} and f_{2a}, respectively. It is worth mentioning that passband response can be greatly affected if any zero gets too close to the resonant peaks. It is interesting to note that f_{2z} and f_{3z} merge together at certain θ_S point, and so f_{4z} and f_{5z} do.

Figure 5 plots the simulated $|S_{21}|$ responses in the first and the second bands using the software package IE3D [23], for the circuit with $Z_1 = 80\,\Omega$, $Z_2 = 25.3\,\Omega$ and $Z_3 = 55.8\,\Omega$ and $\phi_1 = \phi_2 = 0$ for $\theta_S = 90°$, $112.5°$ and $135°$. The substrate has $\varepsilon_r = 10.2$ and thickness $= 1.27\,\text{mm}$. The feed lines are separated from the ring by a small gap. When $\theta_S = 90°$, the two peaks in the first band have a similar $|S_{21}|$ level. It will lead to a symmetric passband. In the second band, however, only one peak exists since f_{2b} is suppressed by f_{3z}, as validated by Fig. 4. When the separation angle $\theta_S = 135°$, the two peaks in the second band have a similar $|S_{21}|$ level, but there is no transmission zero near
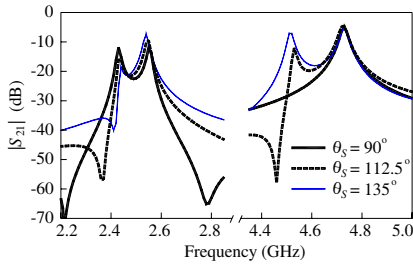
Figure 5. Test of $|S_{21}|$ responses for the ring resonator filter with $N = 8$. (a) f_1. (b) $|S_{21}|$ at f_2. $Z_1 = 80\,\Omega$, $Z_2 = 25.3\,\Omega$.

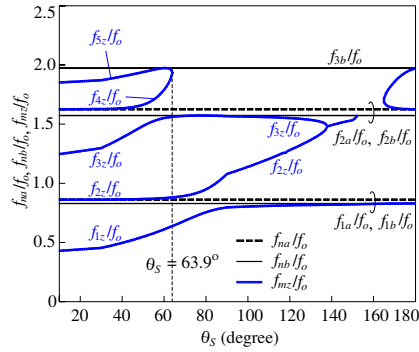**Figure 6.** Transmission zero design graph for the resonator with $N = 6$. $R = 3$, $R' = 3.6$.

the passband. When $\theta_S = 112.5°$, the level differences between the two peaks in both bands are less than $7\,\text{dB}$. Note that in this case each lower peak is neighboring with a transmission zero. Thus, both passbands may have an asymmetric response when the two peaks have identical input and output coupling [6].

Figure 6 shows the resonances f_{na} and f_{nb} and zeros f_{mz} against θ_S for the resonator with $N = 6$. Notice that f_{3a} is not shown since it is far away from f_{3b} (See also Fig. 2).

4. SIMULATION AND MEASUREMENT

4.1. Dual-mode Dual-band Ring Resonator Filter with $N = 8$

Figure 7(a) plots the simulated and measured results of the proposed dual-mode dual-band filter with $\theta_S = 112.5°$. It is designed to have $f_1 = 2.5\,\text{GHz}$ and $f_2 = 4.72\,\text{GHz}$ and fractional bandwidths $\Delta_1 = 6.04\%$ and $\Delta_2 = 5.51\%$. The circuit parameters are the same as those used in Fig. 3. The corresponding line widths for the sections Z_1, Z_2 and Z_3, are 0.36, 3.80 and $0.93\,\text{mm}$, respectively. The outer radius of the ring is $5.78\,\text{mm}$ and the area occupied by the circuit is only 58.3% of a conventional dual-mode ring filter operating at f_1. The gap size between the line-to-ring coupler and the ring is $0.15\,\text{mm}$, and $\phi_1 = 51°$ and $\phi_2 = 39°$. The line-to-ring coupler has to support the two passbands simultaneously.

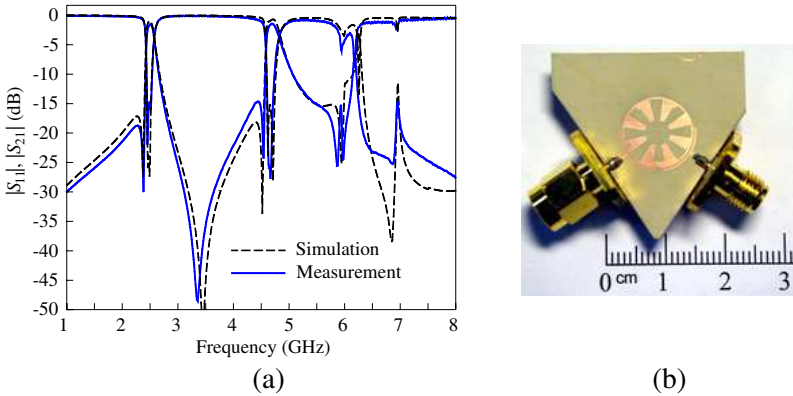The patches Z_p are used to trim the bandwidths. As shown in

Figure 7. (a) Simulated and measured $|S_{11}|$ and $|S_{21}|$ responses. (b) Photograph of the test circuit. $R = 3$, $R' = 0.5R$.

Fig. 5, the distance between the two peaks at f_2 is larger than that at f_1, so it needs more coupling. In this case, however, stronger coupling with larger ϕ_1 and ϕ_2 will cause the response at f_1 to be over-coupled. Thus, the patches are added at virtual short-circuited positions for the even mode resonance at f_2, leading to a shorter distance between the two peaks so that the required coupling level needs no more increment. At the same time, these positions are the open circuit points for the resonances at f_1. The patches bring both resonances at f_1 to shift down together, but the change of bandwidth is negligible. The size of Z_p is $0.5 \times 0.37\,\mathrm{mm}^2$.

In Fig. 7(a), the measured the insertion losses are $1.9\,\mathrm{dB}$ and $1.5\,\mathrm{dB}$ and return losses are better than $18\,\mathrm{dB}$ and $15\,\mathrm{dB}$ at f_1 and f_2, respectively. The four transmission zeros are at $2.42\,\mathrm{GHz}$, $3.5\,\mathrm{GHz}$, $4.55\,\mathrm{GHz}$ and $5.85\,\mathrm{GHz}$, offering good transition responses. The first spurious in the upper rejection band occurs at $6.3\,\mathrm{GHz}$, which is close to the theoretical value (point A) in Fig. 3. Fig. 7(b) shows the photograph of the experimental circuit.

4.2. Dual-mode Dual-band Ring Resonator Filter with $N = 6$

A similar design procedure can be applied to this dual-mode dual-band circuit. A study of the resonator with $N = 6$ like that in Fig. 3 shows that the frequency ratio f_2/f_1 is between 1.8 and 2.0. As shown in Fig. 2, the resonant frequency f_{3a} is much larger than f_{3b}, a wider upper stopband can be achieved if the resonance at f_{3b} can be suppressed. This can be done by allocating the zero f_{5z} very close to it, leading

to the separation between the input and output $\theta_S = 62.5°$, as shown by the dashed line in Fig. 6. The line width and gap size of line-to-ring structure are 0.2 mm. The radius of the ring is 5.67 mm, and its normalized area is 57.2%.

Figure 8(a) presents the simulated and measured results. The circuit has $f_1 = 2.49$ GHz and $f_2 = 4.77$ GHz with fractional bandwidths $\Delta_1 = 8.11\%$ and $\Delta_2 = 4.54\%$. The measured $|S_{21}|$ at f_1 and f_2 are 2.39 dB and 2.2 dB, respectively, and $|S_{11}|$ at both frequencies are better than 15 dB. The two pairs of zeros located at both sides of passbands are 1.93 GHz, 2.57 GHz, 4.35 GHz and 5.49 GHz. Since f_{3b} is totally suppressed by f_{5z}, the circuit demonstrates an improved upper stopband performance as compared with the previous filter with $N = 8$. Again, two Z_p patches are incorporated into the circuit for tuning the passbands. The measured data show reasonably good agreement with the simulation. Fig. 8(b) shows the photograph of the test circuit.

4.3. Dual-mode Dual-band Ring Resonator Filter with $N = 4$

Again, the second resonances of this ring resonator are not degenerate, and f_{2a} is far away from f_{2b} as shown in Fig. 2. This introduces a challenge to synthesis of the second passband. To tackle this problem, extra open stubs (width W and length ℓ) are incorporated into the design. The idea for adding these stubs is similar to the addition of the
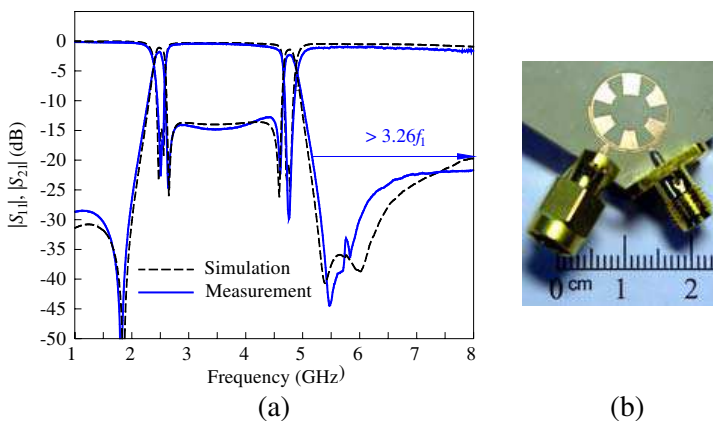

(a)   (b)

Figure 8. Performance of the filter with $N = 6$. (a) Simulated and measured results. (b) Photograph of the experimental circuit. Circuit parameters: $Z_1 = 91.3\,\Omega$, $Z_2 = 30.4\,\Omega$, $Z_3 = 27.3\,\Omega$, $Z_p = 0.62 \times 0.26\,\text{mm}^2$, $\phi_1 = 27°$, and $\phi_2 = 63°$.

Z_p patches for the previous filters with $N = 8$ and 6. Fig. 9(a) draws
the circuit layout, showing that the stubs are attached to the middle of
the Z_1-section and have a space angle of $45°$ away from the plane PQ.
Consider the lower-right quarter of the ring. The resonances f_{2a} and f_{2b}
are the natural frequencies of a stepped-impedance (Z_2-Z_1-Z_2) section
when the centers of the Z_2 sections are short-circuited and open circuit,
respectively. Thus, the center of Z_1 is a virtual ground point at f_{2b},
and an open circuit point at f_{2a}. Attaching any stub to this point will
not alter f_{2b} but will bring f_{2a} down to lower frequencies, depending
on the lengths of the stubs [24]. Here, two stubs, rather than four for
all the centers of the Z_1-sections, are sufficient for the frequency tuning
purpose. Fig. 9(b) is the photograph of the experimental circuit.
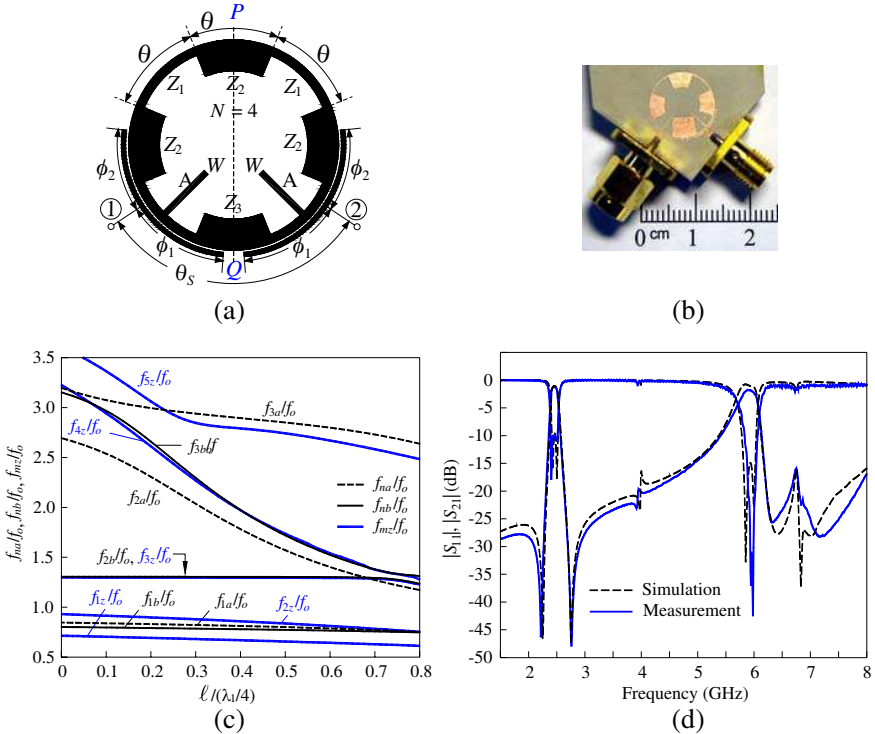

Figure 9. Performances of dual-mode dual-band filter with $N = 4$.
(a) Circuit layout. (b) Photograph of the experimental circuit. (c)
Variations of f_{na}, f_{nb} and f_{mz} with respect to the stub length.
$W = 0.2$ mm. (d) Simulated and measured results. $\ell = 3.6$ mm.
Circuit parameters: $Z_1 = 91.3\,\Omega$, $Z_2 = 30.4\,\Omega$, $Z_3 = 25\,\Omega$, $\phi_1 = 40°$,
and $\phi_2 = 40°$.

Figure 9(c) plots the resonant peaks f_{na}, f_{nb} and transmission zeros f_{mz} versus the normalized length $\ell/(\lambda_1/4)$, where λ_1 is the guided wavelength of a uniform ring resonator with line impedance Z_1 at f_1. Here, the $\theta_S = 90°$ is used. It is worth mentioning that these results are obtained by direct computation based on the transmission-line theory, as those in Figs. 3, 4 and 6. One can see that f_{2a} and f_{3b} shift down rapidly to lower frequencies as $\ell/(\lambda_1/4)$ is increased. This is because at the f_{2a} and f_{3b} resonances the open stubs are attached to the positions where maximal voltages occur. Note that f_{2b} does not change when $\ell/(\lambda_1/4)$ is changed, and that f_{2b} is collocated with f_{3z} since $\theta_S = 90°$ is used. It is worth mentioning that the two resonances and the two zeros of the first passband decrease slowly and simultaneously when ℓ is increased, and that $f_{4z} > f_{3b}$ when $\ell/(\lambda_1/4) < 0.08$ or $\ell/(\lambda_1/4) > 0.375$.

Figure 9(d) plots the simulated and measured results of the proposed circuit. The $\ell/(\lambda_1/4)$ here is selected as 0.4. Note that f_{1a} and f_{1b} support the first passband and f_{2a} and f_{3b} establish the second one. The later two resonances are non-degenerate modes. The circuit has $f_1 = 2.47\,\text{GHz}$ and $f_2 = (f_{2a} + f_{3b})/2 = 5.83\,\text{GHz}$ with $\Delta_1 = 5.39\%$ and $\Delta_2 = 7.07\%$, respectively. Note that the ratio $f_2/f_1 = 2.36 > 2$. The measured $|S_{11}|$ and $|S_{21}|$ are $-10.2\,\text{dB}$ and $-1.6\,\text{dB}$ at f_1 and $-31.1\,\text{dB}$ and $-2.18\,\text{dB}$ at f_2. Two zeros located at both sides of the first band are $2.25\,\text{GHz}$ and $2.69\,\text{GHz}$. The $|S_{21}|$ glitch around $4\,\text{GHz}$ confirms the fact that f_{2b} is suppressed by f_{3z}. The peak at $6.75\,\text{GHz}$ is f_{3a}, which is $2.8f_1$ and has about 7% error compared with the curve shown in Fig. 9(c). The deviation could be due to the parasitic effects of the impedance junctions which are not taken into the account in the transmission line theory. The measured passband responses have good agreement with the simulation. The circuit uses 62% of the area of a conventional ring filter at f_1. The circuit operates at $2.4/5.8$ GHz, showing very suitable for the WLAN applications.

5. CONCLUSION

Dual-mode dual-band bandpass filters are realized with a single periodic stepped-impedance ring resonator. Resonant properties of the resonators for use in dual-band design are investigated. A transmission zero design graph is proposed to facilitate the filter synthesis. With the aids of this graph, two transmission zeros on both sides of each passband can be well planned before the circuit is realized. All designs of ring resonator bandpass filters can be benefited by this graph, which can be established by the transmission line theory. Three filters are realized and their performances are compared with the simulation. The filter with $N = 8$ demonstrates sharp transition and good rejection

performances between the two passbands. The circuit carried out with $N = 6$ shows an improved upper stopband.

In the design with $N = 4$, extra open stubs are incorporated to achieve the dual-mode property in the two passbands. The major drawback of rings with $N = 6$ and 8 for design of dual-band circuit is the narrow ratio range of the second to the first operation frequency. However, it can be significantly extended by using the shunt open stubs, as shown for the case with $N = 4$. All the realized circuits occupy only about 60% of area a traditional ring filter at the first frequency. The measured responses show good agreement with the simulated results.

ACKNOWLEDGMENT

REFERENCES

1. Chang, K. and L.-H. Hsieh, *Microwave Ring Circuits and Related Structures*, Wiley, New Jersey, NY, 2004.
2. Mo, S.-G., Z.-Y. Yu, and L. Zhang, "Design of triple-mode bandpass filter using improved hexagonal loop resonator," *Progress In Electromagnetics Research*, Vol. 96, 117–125, 2009.
3. Zhu, L. and K. Wu, "A joint field/circuit model of line-to-ring coupling structures and its application to the design of microstrip dual-mode filters and ring resonator circuits," *IEEE Trans. Microw. Theory Tech.*, Vol. 47, No. 10, 1938–1948, Oct. 1999.
4. Kundu, A. C. and I. Awai, "Control of attenuation pole frequency of a dual-mode microstrip ring resonator bandpass filter," *IEEE Trans. Microw. Theory Tech.*, Vol. 49, No. 6, 1113–1117, Jun. 2001.
5. Matsuo, M., H. Yabuki, and M. Makimoto, "Dual-mode stepped-impedance ring resonator for bandpass filter applications," *IEEE Trans. Microw. Theory Tech.*, Vol. 49, No. 7, 1235–1240, Jul. 2001.
6. Kuo, J.-T. and C.-Y. Tsai, "Periodic stepped-impedance ring resonator (PSIRR) bandpass filter with a miniaturized area and desirable upper stopband characteristics," *IEEE Trans. Microw. Theory Tech.*, Vol. 54, No. 3, 1107–1112, Mar. 2006.
7. Chiou, Y.-C., J.-T. Kuo, and J.-S. Wu, "Miniaturized dual-mode ring resonator bandpass filter with microstrip-to-CPW broadside-

coupled structure," *IEEE Micow. Wirelss Compon. Lett.*, Vol. 18, No. 2, 97–99, Feb. 2008.

8. Behera, S. and K. J. Vinoy, "Microstrip square ring antenna for dualband operation," *Progress In Electromagnetics Research*, Vol. 93, 41–56, 2009.

9. Alkanhal, M. A. S., "Composite compact triple-band microstrip antennas," *Progress In Electromagnetics Research*, Vol. 93, 221–236, 2009.

10. Heidari, A. A., M. Heyrani, and M. Nakhkash, "A dual-band circularly polarized stub loaded microstrip patch antenna for GPS applications," *Progress In Electromagnetics Research*, Vol. 92, 195–208, 2009.

11. Castaldi, G., V. Fiumara, and I. Gallina, "An exact synthesis method for dual-band Chebyshev impedance transformers," *Progress In Electromagnetics Research*, Vol. 86, 305–319, 2008.

12. Wu, Y., Y. Liu, and S. Li, "A compact pi-structure dual band transformer," *Progress In Electromagnetics Research*, Vol. 88, 121–134, 2008.

13. Kuo, J.-T., T.-H. Yeh, and C.-C. Yeh, "Design of microstrip bandpass filters with a dual-passband response," *IEEE Trans. Microw. Theory Tech.*, Vol. 53, No. 4, 1331–1337, Apr. 2005.

14. Wu, G.-L., W. Mu, X.-W. Dai, and Y.-C. Jiao, "Desing of novel dual-band bandpass filter with microstrip meander-loop resonator and CSRR DGS," *Progress In Electromagnetics Research*, Vol. 78, 17–24, 2008.

15. Wang, X.-H. and B.-Z. Wang, "Compact broadband dual-band bandpass filters using slotted ground structures," *Progress In Electromagnetics Research*, Vol. 82, 151–166, 2008.

16. Chen, J.-X., T.-Y. Yum, J.-L. Li, and Q. Xue, "Dual-mode dual-band bandpass filter using stacked-loop structure," *IEEE Microw. Wireless Compon. Lett.*, Vol. 16, No. 9, 502–504, Sep. 2006.

17. Zhang, X. Y. and Q. Xue, "Novel dual-mode dual-band filters using coplanar-waveguide-fed ring resonators," *IEEE Trans. Microw. Theory Tech.*, Vol. 55, No. 10, 2183–2190, Oct. 2007.

18. Yang, R.-Y., K. Hon, C.-Y. Hung, and C.-S. Ye, "Design of dual-band bandpass filters using a dual feeding structure and embedded uniform uniform impedance resoanators," *Progress In Electromagnetics Research*, Vol. 105, 93–102, 2010.

19. Huang, T.-H., H.-J. Chen, C.-S. Chang, L.-S. Chen, Y.-H. Wang, and M.-P. Houng, "A novel compact ring dual-mode filter with adjustable second-passband for dual-band applications," *IEEE*

Microw. Wireless Compon. Lett., Vol. 16, No. 6, 360–362, Jun. 2006.

20. Chiou, Y.-C., C.-Y. Wu, and J.-T. Kuo, "New miniaturized dual-mode dual-band ring resonator bandpass filter with microwave C-sections," *IEEE Microw. Wireless Compon. Lett.*, Vol. 20, No. 2, 67–69, Feb. 2010.

21. Luo, S. and L. Zhu, "A novel dual-mode dual-band bandpass filter based on a single ring resonator," *IEEE Microw. Wireless Compon. Lett.*, Vol. 19, No. 8, 497–499, Aug. 2009.

22. Luo, S., L. Zhu, and S. Sun, "A dual-band ring-resonator bandpass filter based on two pairs of degenerate modes," *IEEE Trans. Microw. Theory Tech.*, Vol. 58, No. 8, Aug. 2010.

23. *IE3D Simulator*, Zeland Software Inc., Jan. 1997.

24. Chiou, Y.-C. and J.-T. Kuo, "Comment on 'Compact UWB bandpass filter using stub-loaded multiple-mode resonator'," *IEEE Microw. Wireless Compon. Lett.*, Vol. 17, No. 11, 811, Nov. 2007.